

samples. For instance, the 45% C₁/PMMA sample appears to have a T_g about 25 °C higher than the C₂ sample of the same concentration. The high melting temperature of the neat C₁ and the endothermic peak detected in the DSC thermogram of the 60% C₁/PMMA sample near this temperature (see Figure 2b) also indicate that C₁ might be prone to forming solidlike dimers or higher aggregates in the PMMA.

The RRD model combined with the local viscosity and hydrodynamic scaling theories gives a consistent explanation of the τ_f^m at high T and high solvent concentrations. At low solvent concentrations and low T the environment of a solvent molecule differs strongly from that in the neat liquid so that the scaling laws predicted by this simple theory are no longer obeyed.

Acknowledgment. This work was supported by NSF Grant CHE85-11178 to R.P., the NSF MRL Program through the Center for Materials Research at Stanford University, and the IBM Corp.

Registry No. PMMA, 9011-14-7; methyl *p*-chlorobenzoate, 1126-46-1; ethyl *p*-chlorobenzoate, 7335-27-5; propyl *p*-chlorobenzoate, 25800-30-0; butyl *p*-chlorobenzoate, 27942-64-9; pentyl *p*-chlorobenzoate, 97222-04-3.

References and Notes

- (1) Park, J.-K.; Pecora, R.; Ouano, A. C. *Macromolecules*, preceding paper in this issue.

- (2) Kivelson, D.; Madden, P. A. *Annu. Rev. Phys. Chem.* **1980**, *31*, 523.
- (3) Ouano, A. C.; Pecora, R. *Macromolecules* **1980**, *13*, 1167, 1173.
- (4) Oliver, N. H.; Pecora, R.; Ouano, A. C. *Macromolecules* **1985**, *18*, 2208.
- (5) Patterson, G. D.; Lindsey, C. P.; Stevens, J. R. *J. Chem. Phys.* **1979**, *70*, 643.
- (6) Vekslil, Z.; Miller, W. *Macromolecules* **1977**, *10*, 686, 1245.
- (7) Jackson, D. A.; Pike, E. R.; Powles, J. G.; Vaughn, J. M. *J. Phys. C: Solid State Phys.* **1973**, *6*, L55.
- (8) Wang, C. C.; Pecora, R. *J. Chem. Phys.* **1980**, *72*, 5333.
- (9) Perrin, F. *J. Phys. Radium* **1934**, *5*, 497; **1936**, *7*, 1.
- (10) Tirado, M. M.; Garcia de la Torre, J. *J. Chem. Phys.* **1979**, *71*, 2581; **1980**, *73*, 1986.
- (11) Litt, M. H. *Trans. Soc. Rheol.* **1976**, *20*, 47.
- (12) Sugden, S. *J. Chem. Soc.* **1927**, 1786.
- (13) Starkweather, H. W. *Macromolecules* **1975**, *8*, 476.
- (14) Barrer, R. M.; Barrie, J. A. *J. Polym. Sci.* **1957**, *23*, 315.
- (15) Yasuda, H.; Stannett, V. *J. Polym. Sci.* **1962**, *57*, 907.
- (16) Starkweather, H. W. In *Structure Solubility Relationship in Polymers*, Harris, F. W., Seymour, R. B., Eds.; Academic: New York, 1977.
- (17) Kirkwood, J. G.; Buff, F. P. *J. Chem. Phys.* **1951**, *19*, 774.
- (18) Zimm, B. H. *J. Chem. Phys.* **1953**, *21*, 934.
- (19) Misra, A.; David, D. J.; Snelgrove, J. A.; Matis, G. *J. Appl. Polym. Sci.* **1986**, *31*, 2387.
- (20) Bristow, G. M.; Watson, W. F. *Trans. Faraday Soc.* **1958**, *54*, 1742.
- (21) Fox, T. G. *Polymer* **1962**, *3*, 71, 111.
- (22) Alms, G. R.; Bauer, D. R.; Brauman, J. I.; Pecora, R. *J. Chem. Phys.* **1973**, *59*, 5310, 5321. Bauer, D. R.; Brauman, J. I.; Pecora, R. *J. Am. Chem. Soc.* **1974**, *96*, 6840.
- (23) Evans, G. T.; Kivelson, D. *J. Chem. Phys.* **1986**, *84*, 385.

Structure and Dynamics of Epoxy Polymers

Benjamin Chu* and Chi Wu

Chemistry Department, State University of New York at Stony Brook, Long Island, New York 11794-3400. Received September 10, 1987; Revised Manuscript Received November 12, 1987

ABSTRACT: Laser light scattering and small-angle X-ray scattering (SAXS) studies have been made of the curing of epoxy resins from 1,4-butanediol diglycidyl ether with *cis*-1,2-cyclohexanedicarboxylic anhydride. The epoxy resin before its gel point is soluble in methyl ethyl ketone, and the scattering techniques can be used to determine the molecular weight, the fractal dimension, and the molecular weight distribution of the branched epoxy polymer during each stage of the initial polymerization process. After gelation, SAXS remains a useful technique for studying the branched polymer structure in terms of the concept of fractal geometry for random systems.

I. Introduction

The kinetics and mechanism of copolymerization of epoxide resins with anhydrides or amines, with or without a catalyst, have been of interest because these materials often constitute an important component in reinforced composites. However, the mechanism of the curing reaction of epoxide and anhydrides has been somewhat uncertain as a number of partially conflicting reaction mechanisms have been proposed in recent years.¹ In this paper, we are interested in studying the structure and dynamics of branched epoxy polymer products during different stages of the curing process. By developing a methodology whereby we can examine the details of the branched epoxy polymer structure, we hope to be able to relate properties of some aspects of the microstructure with macroscopic properties of the epoxy resins. Thus, our approach represents only the first phase of our epoxy studies with emphasis on the determination of fundamental macromolecular parameters, such as the weight average molecular weight M_w and the molecular weight

distribution MWD of branched epoxy polymers, and the nature of branched structure in terms of its fractal geometry.² Ultimately, the possibility of in situ determination of such properties before the gel point using the noninvasive scattering techniques will be investigated. In order to avoid complications related to intermolecular interactions, our experiments deal mainly in the dilute solution regime, ignoring at this time studies of structures and dynamics of epoxy resins in concentrated solutions of their own reaction bath. An earlier communication³ has detailed the use of fractal geometry as an application to branched epoxy polymer characterizations.

II. Experimental Methods

1. Materials. 1,4-Butanediol diglycidyl ether (DGEb, $M_w = 202.3$) and *cis*-1,2-cyclohexanedicarboxylic anhydride (CH, $M_w = 154.2$) were purchased from Aldrich Chemical Co. and used without further purification since the same experimental results were obtained when both components were purified by vacuum distillation. The catalyst (CA), benzyldimethylamine ($M_w = 135.2$, courtesy of Gary L. Hagnauer, Polymer Research Division, Army

Table I
Properties of Epoxy Polymer (1,4-Butanediol Diglycidyl Ether with *cis*-1,2-Cyclohexanedicarboxylic Anhydride) during the Curing Process

sample	% CH convn	M_w (g/mol)		$\langle R_g^2 \rangle^{1/2}$ (Å)		A_2 (mL·mol/g ²)	
		X-ray	LLS	X-ray	LLS	X-ray	LLS
1	6.5	4.32×10^3	4.11×10^3	29			1.45×10^{-3}
2	13.3	6.14×10^3	6.07×10^3	36			1.26×10^{-3}
3	20.0	8.23×10^3	8.23×10^3	44		1.05×10^{-3}	1.01×10^{-3}
4	26.5	1.25×10^4	1.22×10^4	55			8.70×10^{-4}
5	33.5	2.11×10^4	2.04×10^4	70			7.41×10^{-4}
6	36.0	3.37×10^4	3.15×10^4	85		6.12×10^{-4}	6.30×10^{-4}
7	38.5	5.60×10^4	5.00×10^4	112	105		5.25×10^{-4}
8	40.0		7.68×10^4		128		4.57×10^{-4}
9	41.0		1.03×10^5		150		4.17×10^{-4}
10	42.5		1.42×10^5		191		3.63×10^{-4}
11	44.0		2.19×10^5		222		3.16×10^{-4}
12	45.3		3.01×10^5		257		2.88×10^{-4}
13	46.5		4.97×10^5		314		2.51×10^{-4}

Materials Technology Laboratory, Watertown, MA) was vacuum distilled before use.

2. Preparation of Solutions. Known weights of CH were heated to $\sim 50^\circ\text{C}$ in order to melt the CH. The melted CH was then cooled to $\sim 37^\circ\text{C}$, a few degrees above the melting point of CH ($\sim 32\text{--}34^\circ\text{C}$), and mixed well with known weights of DGEb. Then, a small amount of catalyst was added to the homogeneous liquid mixture using a Drummond digital microdispenser ($\pm 0.01 \mu\text{L}$). The well-mixed reaction mixture containing a molar ratio of epoxy (DGEb):curing agent (CH):catalyst (CA) = 1:2:0.001 was centrifuged at ~ 18000 gravity and $\sim 38^\circ\text{C}$ for 2 h. A middle portion of the centrifuged reaction mixture was then transferred to dust-free cylindrical light scattering cells of 17-mm o.d. Composition of the reaction mixture during curing could be analyzed chemically.⁴

3. Methods of Measurements. A high-temperature light scattering spectrometer was used for measurements of the angular distribution of absolute scattered intensity as well as its spectral distribution.⁵ The glass jacket (4 in Figure 2 of ref 5) was modified so that the inner brass thermostat (5 in Figure 2 of ref 5) was immersed in a glass jacket containing refractive-index matching oil. This more standard arrangement permitted a reduction in the o.d. of the cylindrical light scattering cell to between 10 and 17 mm and consequent reduction in the solution volume required to carry out light-scattering experiments. With the refractive-index matching oil, we could also cover a broader scattering angular range varying from about 10° to 140° , even though the smaller accessible scattering angular range was relatively unimportant for the epoxy characterizations, especially during the initial curing process. The details of light-scattering instrumentation have been described elsewhere.⁴

We have modified a Kratky block collimation system for small-angle X-ray scattering (SAXS) at the State University of New York (SUNY) X21A2 beamline, National Synchrotron Light Source (NSLS), Brookhaven National Laboratory (BNL). Two linear position sensitive detectors (LPSD) have been adapted to the Kratky small-angle X-ray diffractometer⁶ (SAXD), a Braun LPSD with an effective detector length of ~ 5 cm, and a photodiode array LPSD with an effective detector length of ~ 2.5 cm. For the epoxy polymer studies, we used a slit width of ~ 0.5 mm and covered a K range between ~ 0.07 and $\sim 3.4 \text{ nm}^{-1}$ where the scattering wave vector $\mathbf{K} = (4\pi/\lambda) \sin(\theta/2)$ with λ and θ being an X-ray wavelength of 0.154 nm and the scattering angle, respectively. Two ionization chambers were used to measure the sample transmission. The SAXS curves have been corrected for detector linearity, parasitic scattering, solvent background, and sample attenuation. Desmearing was unnecessary as the incident X-ray beam had a small cross section of 0.5×2 mm at the sample chamber.

III. Results and Discussion

1. Refractive Index Increment Measurements. An absolute determination of the polymer molecular weight requires information on the refractive index increment (dn/dc) as well as the Rayleigh ratio. The refractive index increment was determined according to the procedure

outlined in ref 4. We did not try to isolate the epoxy polymer from varying amounts of unpolymerized DGEb and CH. Instead, we determined dn/dc for the epoxy polymers in methyl ethyl ketone (MEK) in the presence of small amounts of DGEb and CH.

We have taken into account the varying amounts of DGEb and CH by adding corresponding quantities of unreacted DGEb and CH with the solvent MEK in order to keep the ratio of MEK:DGEb:CH constant for the branched epoxy polymer solutions. Thus, for each branched epoxy polymer that we withdrew from the reaction mixture, we dissolved the polymer at different concentrations using a mixed solvent with a constant ratio of MEK:DGEb:CH. Furthermore, we took into account possible solvent preferential interactions by using two different mixed-solvent ratios (MEK:DGEb:CH = 1:0.03:0.025 and 1:0.01:0.007 in volume ratios). The same results (molecular weight and radius of gyration) were obtained. Thus, we do not have to take into account the small variation in the mixed-solvent composition in our analysis. $dn/dc = 0.180 \pm 0.002$ within the above two volume ratios of MEK:DGEb:CH at $\lambda_0 = 488$ nm and 25°C , and the refractive index of the corresponding solvent mixture is 1.377.

2. Light Scattering Intensity Measurements. The excess absolute integrated intensity of light scattered by a dilute polymer solution has the form

$$\frac{HC}{R_{vv}(K)} = \frac{1}{M_w} \left(1 + \frac{K^2 \langle R_g^2 \rangle_z}{3} \right) + 2A_2C \quad (1)$$

where the optical constant $H = (4\pi^2 n^2 / N_A \lambda_0^4) (dn/dc)_T^2$, with λ ($\equiv \lambda_0/n$), A_2 , $\langle R_g^2 \rangle_z^{1/2}$ ($\equiv R_g$), M_w , and K being, respectively, the wavelength of light in the scattering medium, the second virial coefficient, the z -average root-mean-square radius of gyration, the weight-average molecular weight, and the magnitude of the momentum transfer vector. The subscripts vv denote vertically polarized incident and scattered light. From a Zimm plot as shown typically in Figure 1, we can determine M_w , R_g , and A_2 . The results are listed in Table I.

3. Small-Angle X-ray Scattering Measurements. In SAXS, the excess scattered intensity I is governed by electron density (instead of refractive index) differences between the solute and the solvent. We may write

$$\frac{H'I}{I} \approx \frac{1}{M_w} \left(1 + \frac{K^2 \langle R_g^2 \rangle_z}{3} \right) + 2A_2C \quad (2)$$

where the optical constant H in light scattering has been

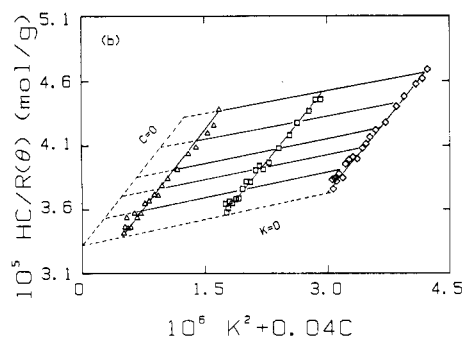


Figure 1. Typical Zimm plot of epoxy polymer in methyl ethyl ketone with traces of unreacted monomers DGEb and CH at 25 °C using light scattering intensity measurements with $\lambda_0 = 488$ nm for sample 12 with $\sim 45.3\%$ CH conversion ($M_w = 3.01 \times 10^5$ g/mol, $A_2 = 2.88 \times 10^{-4}$ mL mol g $^{-2}$, $R_g = 25.7$ nm): (Δ) $C = 1.17 \times 10^{-4}$ g/mL; (\square) $C = 4.27 \times 10^{-4}$ g/mL; (\diamond) $C = 7.54 \times 10^{-4}$ g/mL.

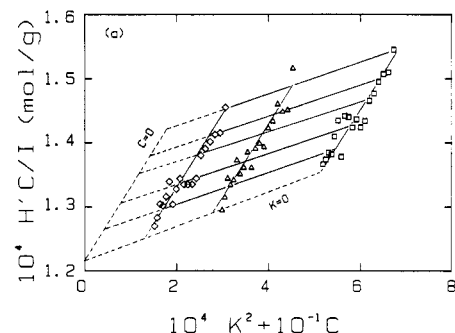


Figure 2. Typical Zimm plot of epoxy polymer in methyl ethyl ketone with traces of unreacted monomers DGEb and CH at 25 °C using small-angle X-ray scattering at the National Synchrotron Light Source ($\lambda = 0.154$ nm, sample 3 with $\sim 20\%$ conversion, $M_w = 8.23 \times 10^3$ g/mol, $A_2 = 1.05 \times 10^{-3}$ mL mol g $^{-2}$, and $R_g = 4.4$ nm): (\circ) $C = 7.89 \times 10^{-4}$ g/mL; (Δ) $C = 1.04 \times 10^{-3}$ g/mL; (\square) $C = 2.51 \times 10^{-3}$ g/mL. $H'C/I$ transfers the light scattering calibration to SAXS by determining the ratio of scattering intensities in light scattering and SAXS of one epoxy polymer solution of known molecular weight.

replaced by an instrument constant H' which takes care of the square effect due to the electron density increment⁷ and instrumentation differences between light scattering and SAXS. Without computing or measuring the electron density increment, we simply determined H' by using an epoxy polymer (sample 3) of known molecular weight (8.23×10^3 g/mol from light scattering measurements) as our SAXS calibration standard. SAXS intensity measurements could then be used to determine M_w , R_g , and A_2 of other epoxy polymer samples^{1,2,4-7} as shown typically in Figure 2. The SAXS results are also listed in Table I. The agreement between light scattering and SAXS results is very good, with M_w values differing by no more than a few percent in most cases. From the initial slopes in plots of $\lim_{C \rightarrow 0} HC/R_{vv}$ and $\lim_{C \rightarrow 0} H'C/I$ versus K^2 , we note that for sample 7, $R_g = 112$ and 105 Å by means of SAXS and light scattering, respectively. An R_g value of ~ 100 Å, as determined by light scattering, has an uncertainty of about 10%, while SAXS with the intense synchrotron X-ray source yields fairly precise R_g values with uncertainties of no more than a few percent down to very small sizes (e.g. R_g (sample 1) = 29 Å). In Figure 2, the unsmoothed excess SAXS intensity has been corrected for detector nonlinearity, sample transmission, solvent background, and parasitic scattering. No desmearing was required because of the small beam cross section and divergence of the incident synchrotron X-ray beam. The agreement of R_g values between light scattering and SAXS also confirms the above assumption over the K range of our measure-

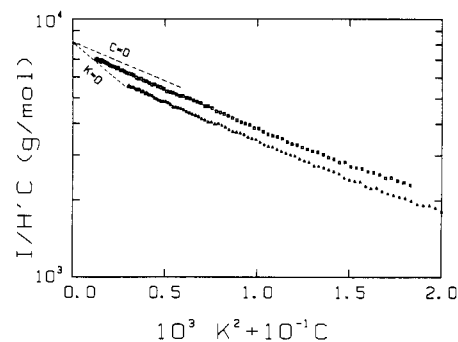


Figure 3. Guinier plots of two of the three concentrations of Figure 2: (\square) $C = 7.89 \times 10^{-4}$ g/mL; (Δ) $C = 2.51 \times 10^{-3}$ g/mL. From the initial slopes, we retrieved essentially the same values for M_w , A_2 , and R_g as stated in Figure 2. The linear behavior in a $\log I$ versus K^2 plot at $KR_g < 1$ in the SAXS measurements is clearly demonstrated.

ments. It should also be noted that the signal-to-noise ratio of our SAXS measurement is better than Figure 2 suggests, as the intensity values have been greatly magnified in order to show the initial slope behavior from the first 19 data points at the lowest scattering angles. If we were to use a conventional X-ray source, we would have great difficulty in achieving such a reciprocal intensity plot. Rather, a Guinier plot of $\log I$ versus K^2 , as shown in Figure 3, represents the standard method of determining R_g . According to eq 2, we have for $C = 0$

$$\begin{aligned} \log(I/H'C) &\approx \log M_w + \log \left(1 - \frac{K^2 R_g^2}{3} \right) \\ &\approx \log M_w - \frac{K^2 R_g^2}{3} \end{aligned} \quad (3)$$

The limiting slope at $C = 0$ and $KR_g \lesssim 1$ yields the radius of gyration. The linear behavior over a much broader K range in SAXS permits a more precise R_g determination for small R_g values ($\lesssim 100$ Å) by means of SAXS when compared with light scattering. In polymer characterization, light scattering and SAXS are truly complementary techniques in covering the size determination. For our epoxy studies, we started with monomers that eventually form very large polymer networks. Thus, during the initial stages of the epoxy polymerization process, SAXS is the proper analytical method to determine R_g of the branched epoxy polymer. Following eq 1 and 3

$$\lim_{C \rightarrow 0} \frac{M_w HC}{R_{vv}(K)} \left(= \lim_{C \rightarrow 0} \frac{M_w H'C}{I(K)} \right) \approx 1 + (R_g/3)K^2 R_g = 1 + (R_g/3)\chi \quad (4)$$

In plots of $\lim_{C \rightarrow 0} M_w HC/R(\theta)$ or $\lim_{C \rightarrow 0} M_w H'C/I$ versus χ ($\equiv K^2 R_g^2$), as shown in Figure 4, we see that laser light scattering (LLS) measurements, as denoted by filled symbols are clearly appropriate for R_g values of a few hundred angstroms. It becomes increasingly more difficult at smaller R_g sizes because of the small KR_g (< 1) ranges accessible to LLS when R_g is very small. For sample 7 (denoted by filled and hollow diamonds) we demonstrate an overlap of two independent scattering techniques on an absolute determination of R_g .

4. Fractal Geometry of Branched Epoxy Polymers.

The curing of epoxy resins from 1,4-butanediol diglycidyl ether (DGEb) with the curing agent *cis*-1,2-cyclohexanedicarboxylic anhydride (CH) in the presence of a small amount of catalyst benzyltrimethylamine (CA) represents a cross-linking polymerization process, as shown schematically in Figure 5. The cross-linking reaction involves

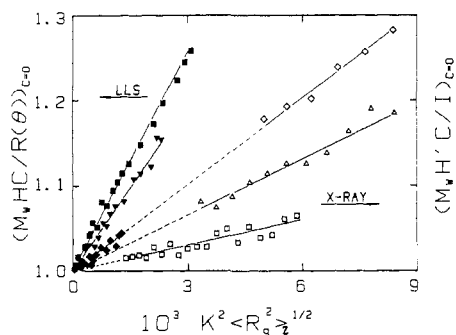


Figure 4. Plots of M_wHC/R_v (for light scattering) and $M_wH'C/I$ (for SAXS) as a function of $K^2\langle R_g^2 \rangle^{1/2}$. According to eq 1 and 3, $\lim_{C \rightarrow 0} M_wHC/R_v (= \lim_{C \rightarrow 0} M_wH'C/I) \cong 1 + \langle R_g^2 \rangle^{1/2}/3K^2 \times \langle R_g^2 \rangle^{1/2}$. Thus, the slope is equal to $\langle R_g^2 \rangle^{1/2}/3$. The plots demonstrate overlapping regions of the two scattering techniques. Laser light scattering is denoted by filled symbols while SAXS is denoted by hollow symbols: (■) sample 12, (▽) sample 10, (◆) sample 7, (◇) sample 7, (△) sample 5, (□) sample 3. Properties of various samples are listed in Table I.

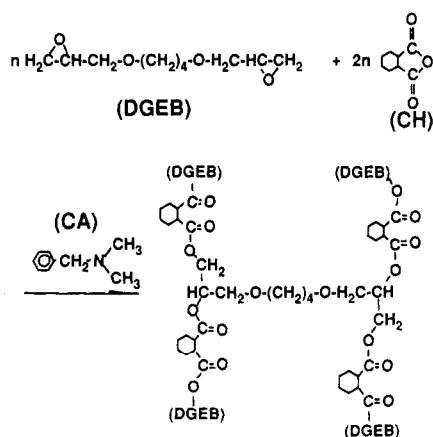


Figure 5. Cross-linking reaction of DGEb with CH in the presence of CA.

roughly n mol of DGEb with $2n$ mol of CH. The chemical reaction is known to cluster at catalytic centers, and the formation of branched structures eventually link together to form loops or polymer networks.

The concept of fractal geometry^{2,8,9} can be a useful tool to describe the branching structure of epoxy polymers during its curing process. The fractal dimension d_R of a molecular cluster with mass M and the radius of gyration has the relation¹⁰ $M \sim R_g^{d_R}$ where d_R is the fractal dimension in terms of the scaling relationship between mass and radius of gyration. For polydisperse polymers, we approximate the expression to be

$$M_w \sim (\langle R_g^2 \rangle^{1/2})^{d_R} \quad (5)$$

In eq 5, we have assumed that the MWDs of branched epoxy polymers are finite and M_w spacings have been sufficiently far apart. It should be noted that polydispersity could act as a simple correction¹⁶ or could affect the measured exponents d_R ¹⁷⁻¹⁹ as well as d_K .^{20,21} However, the linear behavior as shown in Figure 8b, the horizontal region as shown clearly in Figure 9, and our knowledge on the molecular weight distribution as shown in Figure 12 strengthen the supposition of eq 5; i.e., we have a K region with a constant d_K in the "polydisperse" epoxy polymer and d_R can be evaluated over a broad enough M_w range even if the epoxy polymers are "polydisperse." If the branched polymer has a MWD with only a high MW cutoff, the fractal dimension will be scaled even though the scaling relation holds.

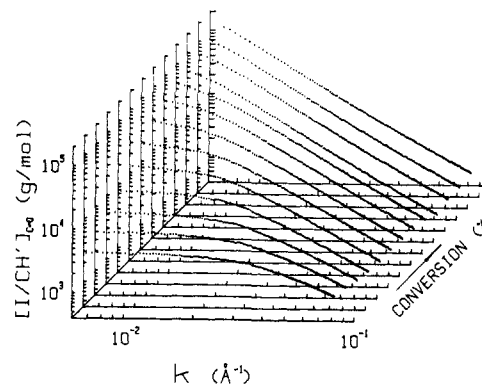


Figure 6. Structure of epoxy polymers as a function of percent CH conversion. $[I/CH]_{C=0}$ represents absolute SAXS intensity at infinite dilution in units of g/mol. Thus, $\lim_{K \rightarrow 0} [I/CH]_{C=0} = M_w$. The scattering curves are numbered with increasing percent CH conversion. Properties of the 13 samples representing epoxy polymers during different stages of the curing process are listed in Table I.

The two-point density-density correlation function $C(r)$ has the form¹¹ $C(r) \cong C_0 r^{-\alpha}$ with the corresponding static structure factor $S(K)$ (\sim the scattered intensity I), which is the Fourier transform of the pair correlation function, having a power-law relation

$$S(K) \sim K^{-d_K} \quad (6)$$

The fractal dimension d_K is related to the exponent α according to $d_K = d - \alpha$ with d being the dimensionality of the embedding space or lattice containing the fractal. For a self-similar fractal $d_f = d_K = d_R$ where d_f is a general fractal dimension.¹² Measurements of the angular distribution of scattered intensity over large ranges of K with $R_g^{-1} < K < \xi^{-1}$ permit us to determine d_K according to eq 6 where ξ is a correlation length related to the "blob" size. Measurements of M_w and R_g of the epoxy polymer by means of Zimm plots during the polymerization process permit us to determine d_R according to eq 5. In this section, our main aim is to check eq 5 and 6 and to find out if our epoxy polymers form self-similar fractals.

Figure 6 shows static structure factors $S(K) [= I/CH]$ from SAXS as a function of percent CH conversion. In plotting the scattering curves, we have scaled the intensities according to eq 3. Thus, the y ($\equiv \lim_{C \rightarrow 0} I/CH$) axis has units of g/mol and at $K = 0$ denotes the M_w of the epoxy polymer as a function of percent CH conversion. Such an approach is feasible up to the gelation point, beyond which the epoxy polymer can no longer be dissolved as individual macromolecules in MEK. At high percent CH conversion, the epoxy polymer has reached fairly high molecular weights ($\sim 10^5$ g/mol). Thus, SAXS measures mainly the fractal geometry of the branched epoxy polymers in solution according to eq 6, as shown typically in Figure 7 by the hollow diamonds for sample 13 with a M_w of 5×10^5 g/mol. In Figure 7, we have also included LLS measurements (also denoted by hollow diamonds) at much smaller values of K ($< 4 \times 10^{-3} \text{ \AA}^{-1}$). It may be difficult to see from Figure 7 that the initial slope from LLS exhibiting almost horizontal behavior could easily determine the R_g value as has been demonstrated by Figure 1. As the K range covered by SAXS is extremely broad, i.e., down to monomer dimensions, we would also expect a deviation from the fractal dimension beyond $2/R_g \leq K \leq 1/20 \text{ \AA}^{-1}$, i.e., $20K \lesssim 1$ with K expressed in \AA^{-1} . Sample 13 represents the epoxy polymer structure just before its gelation point. At earlier times, e.g. for sample 7 with $M_w = 5 \times 10^4$ g/mol at 38.5% CH conversion, the initial slope from SAXS and that from LLS (both denoted

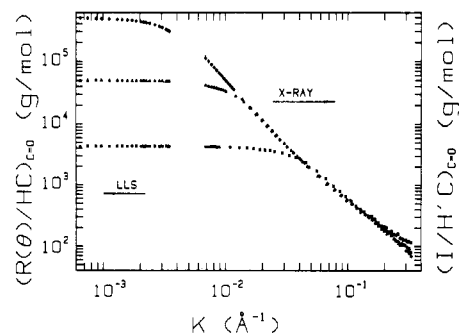


Figure 7. log-log plots of R/HC for light scattering and $I/H'C$ for SAXS as a function of K : (\square) sample 1, (\blacktriangle) sample 7, (\diamond) sample 13. Light scattering K range: $\sim 7 \times 10^{-4} < K < 4 \times 10^{-3} \text{ \AA}^{-1}$. SAXS K range: $7 \times 10^{-3} < K < 3.5 \times 10^{-1} \text{ \AA}^{-1}$. Each SAXS curve has 817 data points, of which only a fraction is plotted. The horizontal portion of the scattering curve with a small initial negative slope can be related to the radius of gyration. In the range $2/R_g \leq K \leq 1/20 \text{ \AA}^{-1}$, we can use the scattering curves to examine fractal geometry of the epoxy polymers.

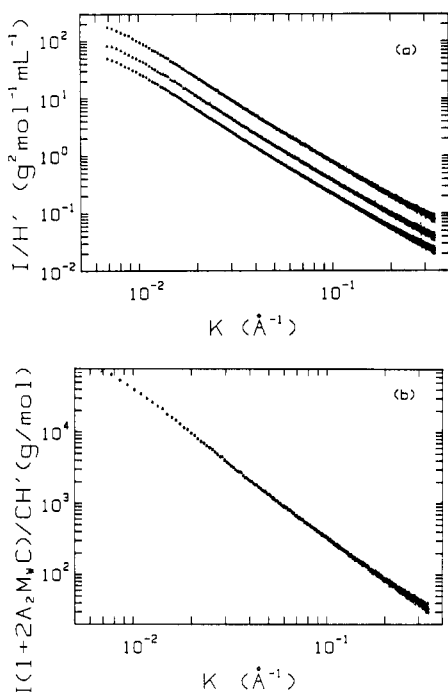


Figure 8. Concentration effect on fractal dimension of epoxy polymers. (a) log-log plots of I/H' versus K for sample 10 in MEK: (\diamond) $C = 7.19 \times 10^{-4} \text{ g/mL}$; (\blacktriangle) $C = 1.14 \times 10^{-3} \text{ g/mL}$; (\blacksquare) $C = 2.41 \times 10^{-3} \text{ g/mL}$. There are 817 data points on each scattering curve. Only a fraction of data points is plotted. (b) log-log plot of a scaled intensity curve based on the scattering curves from three different concentrations as shown in Figure 8a. Same symbols as in Figure 8a with $M_w = 1.42 \times 10^5 \text{ g/mol}$ and $A_2 = 3.63 \times 10^{-4} \text{ mL mol g}^{-2}$. Again only a small fraction of data points is plotted.

by solid triangles) in Figure 7 could be used to determine R_g . The log-log plot of Figure 7 also demonstrates the precision with which we have to achieve in order to measure R_g of the order of 100 Å. The LLS portion of the solid triangles is almost horizontal. We have also included sample 1 (denoted by hollow squares) representing only a 6.5% CH conversion in Figure 7. For sample 1, R_g ($\sim 29 \text{ \AA}$) is no longer accessible by LLS. In the SAXS region, the initial horizontal curve can be used to determine both M_w and R_g . Again, we can use eq 6 to determine the fractal dimension over an appropriate K range ($2/R_g \leq K \leq 1/20 \text{ \AA}^{-1}$). More importantly, we note that the scattering curves of samples 7 and 13 overlap over a broad K range ($1.5 \times 10^{-2} \leq K \leq 3 \times 10^{-1} \text{ \AA}^{-1}$) while the scattering curve for

Table II
(a) Fractal Dimension d_f of Epoxy Polymer Solutions Based on $I(K) \sim K^{d_K}$ of Eq 6 with $(2/R_g) < K < Y$ and (b) Coil Behavior of Epoxy Polymers between the Mesh Points Based on $I(K) \sim K^{-\beta}$ with $Y < K < (1/4) \text{ \AA}^{-1}$

Section a				
sample	d_f			
	$Y^{-1} = 30 \text{ \AA}$	$Y^{-1} = 20 \text{ \AA}$	$Y^{-1} = 15 \text{ \AA}$	$Y^{-1} = 10 \text{ \AA}$
13	2.17 ± 0.01	2.16 ± 0.01	2.14 ± 0.02	2.10 ± 0.03
12	2.17 ± 0.01	2.17 ± 0.02	2.13 ± 0.03	2.11 ± 0.04
11	2.18 ± 0.02	2.17 ± 0.02	2.14 ± 0.02	2.12 ± 0.03
10	2.18 ± 0.01	2.17 ± 0.01	2.15 ± 0.02	2.12 ± 0.02
9	2.17 ± 0.02	2.17 ± 0.02	2.14 ± 0.03	2.10 ± 0.03
8	2.17 ± 0.05	2.16 ± 0.03	2.13 ± 0.03	2.10 ± 0.04
7	2.18 ± 0.05	2.17 ± 0.04	2.14 ± 0.04	2.11 ± 0.05
6	2.16 ± 0.05	2.17 ± 0.04	2.13 ± 0.04	2.09 ± 0.05
5	2.15 ± 0.07	2.16 ± 0.05	2.13 ± 0.04	2.10 ± 0.05
4		2.12 ± 0.06	2.10 ± 0.05	2.05 ± 0.06
3		2.05 ± 0.08	2.00 ± 0.06	1.94 ± 0.06
2			2.04 ± 0.08	1.96 ± 0.07
1				1.90 ± 0.08

Section b				
sample	β			
	$Y^{-1} = 30 \text{ \AA}$	$Y^{-1} = 20 \text{ \AA}$	$Y^{-1} = 15 \text{ \AA}$	$Y^{-1} = 10 \text{ \AA}$
13	1.74 ± 0.06	1.67 ± 0.05	1.64 ± 0.06	1.59 ± 0.09
12	1.76 ± 0.05	1.69 ± 0.05	1.65 ± 0.07	1.61 ± 0.09
11	1.75 ± 0.06	1.67 ± 0.05	1.63 ± 0.07	1.60 ± 0.09
10	1.74 ± 0.05	1.68 ± 0.06	1.67 ± 0.07	1.65 ± 0.10
9	1.73 ± 0.06	1.67 ± 0.05	1.65 ± 0.07	1.62 ± 0.10
8	1.74 ± 0.06	1.68 ± 0.06	1.66 ± 0.07	1.63 ± 0.10
7	1.72 ± 0.07	1.67 ± 0.06	1.65 ± 0.07	1.62 ± 0.09
6	1.71 ± 0.07	1.68 ± 0.06	1.66 ± 0.05	1.62 ± 0.10
5	1.70 ± 0.06	1.68 ± 0.06	1.65 ± 0.06	1.61 ± 0.10
4	1.68 ± 0.07	1.67 ± 0.07	1.65 ± 0.07	1.60 ± 0.10
3	1.68 ± 0.06	1.67 ± 0.07	1.64 ± 0.06	1.58 ± 0.11
2	1.67 ± 0.08	1.68 ± 0.07	1.66 ± 0.07	1.59 ± 0.10
1	1.65 ± 0.08	1.67 ± 0.07	1.66 ± 0.07	1.59 ± 0.11

sample 1 with $M_w = 4 \times 10^3 \text{ g/mol}$ does not overlap with the other two scattering curves even in a log-log plot, indicating structural differences for the epoxy polymer between the very initial stages and before the gelation. We shall return to this point later. In Figure 7, the scattering curves have similar shapes and we want to again emphasize the complementary aspect of the two scattering techniques. For our epoxy polymerization process, we need both LLS and SAXS in order to cover the appropriate K ranges.

Now we turn our attention to the two main tasks, i.e., experimental determinations of d_K and d_R . For d_K , we can determine a value for each sample. However, for d_R , instead of doing a tedious fractionation of each polymer sample, we have chosen the approximate eq 5 and made an experimental determination of M_w and R_g for the epoxy polymer at 13 time intervals up to the neighborhood of the gelation threshold during the curing process.

In the d_K determination, we have considered the concentration effect as follows. Figure 8a shows log-log plots of I/H' versus K for sample 10 in MEK at $C = (\diamond) 7.19 \times 10^{-4} \text{ g/mL}$, (Δ) $1.14 \times 10^{-3} \text{ g/mL}$, and (\blacksquare) $2.41 \times 10^{-3} \text{ g/mL}$. As we have a total of 817 data points for each scattering curve, only a fraction of the data is plotted. It should be noted that the scattering curves are slightly curved. Figure 8b shows a log-log plot of scaled scattered intensities of the three scattering curves of Figure 8a. Overlapping of the three scattering curves with zero adjustable parameters is clearly demonstrated. The results for d_K , as well as the exponent β related to the coil behavior between the entanglement points, are listed in Table II. It should be noted that our d_K values represent the fractal dimension of swollen branched epoxy polymers in solution. The variable Y in Table II represents a correlation length

Table III
Determination of ξ Based on Plots of $\log(W_{\text{measd}}/W_{\text{calcd}})$ versus $\log K^a$

sample	3 ^b	4 ^b	5	6	7	8	9	10	11	12	13
ξ (Å)	18.4 ± 4.7	18.5 ± 4.8	18.9 ± 3.9	20.3 ± 3.7	19.2 ± 3.0	20.1 ± 3.4	18.9 ± 4.2	19.5 ± 3.3	20.0 ± 3.5	20.0 ± 3.4	19.7 ± 3.0

^a ξ^{-1} is determined by the intercept between $W_{\text{measd}}/W_{\text{calcd}} = 1$ and the straight line with slope ≈ 0.49 . ^b Estimated value.

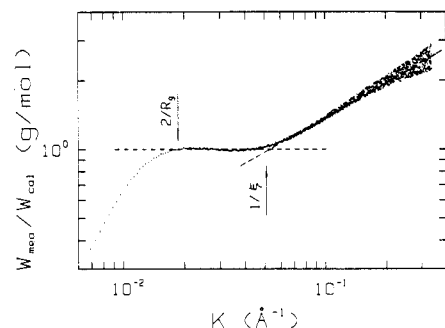


Figure 9. Plot of $W_{\text{measd}}/W_{\text{calcd}}$ versus K for sample 7. $M_w = 5.00 \times 10^4$ g/mol, $R_g = 105$ Å, $W_{\text{measd}} = (I/H^2C)_{\text{measd}, C=0}$, $W_{\text{cal}} = 3.01K^{2.17}$, and slope (at $K > 1/\xi$) = 0.49 ± 0.06 .

ξ below which the polymer coil behavior should begin to dominate. On the basis of the values of constant d_f , we see a cut off value of $Y^{-1} \approx 20$ Å with $d_K \approx 2.17$ for samples 6–13. At earlier polymerization stages, we consider the branched polymer chains to have lower d_f values with ξ no longer related closely to the polymer mesh size. Figure 9 shows a more quantitative approach to determine the mesh size ξ ($\approx 19.2 \pm 3.0$ Å) and to show the deviation of the measured curve from $W_{\text{cal}}(\text{g/mol}) = 3.01K^{2.17}$ with K expressed in Å^{-1} for sample 7. The results are listed in Table III. As the K range obeying the fractal dimension d_K is limited, the range of K used in the determination of d_K should always be considered with care.

Beyond the mesh size range ($K > \xi^{-1}$), we have noted an epoxy polymer coil behavior with $I(K) \sim K^{-\beta}$ and $\beta \approx 1.68 \pm 0.06$, as listed in Table IIb. The value $(d_f - \beta) = 2.17 - 1.68 = 0.49$ is the slope shown in Figure 9 for $K > \xi^{-1}$. Daoud and Joanny¹³ predicted a linear blob behavior of $\beta \sim 5/3$ in a θ solvent.

We now come to the determination of d_R . A log-log plot of $\langle R_g^2 \rangle_z^{1/2}$ versus M_w , as shown in Figure 10, reveals a slight curvature in the low molecular weight region; i.e., during the initial stages of the curing process, the epoxy polymer appears to have different structures from those at later stages even before the gelation threshold. The experimental results shown in Figure 10 required a combination of SAXS (denoted by solid squares) and LLS (denoted by hollow squares) measurements. However, the agreement between the two techniques has been excellent. Furthermore, the curvature is mainly in the SAXS region. Although a least-squares fitting of all the data points using $\langle R_g^2 \rangle_z^{1/2} = k_R M_w^{\alpha_R}$ with $d_R = 1/\alpha_R$ shows a reasonable $d_R = 2.0$, we have approximated the slight curvature at low R_g values by breaking the curve into two straight sections near $M_w \sim 1 \times 10^4$ g/mol. Least-squares fitting of the first three and four low M_w data points yields $d_R \approx 1.55$ and 1.61, respectively, while $d_R (= d_f) \sim 2.05$. Thus, we cannot apply the concept of self-similar fractals in the very beginning of the curing process for our epoxy system.

It is interesting to note that the difference in scattering curves for low molecular weight and for high molecular weight epoxy polymers appears to occur at a fairly high molecular weight of $\sim 10^4$ g/mol. We speculate that the reason for this behavior is due to the relatively low catalyst concentration of $\sim 0.1\%$; i.e., there is only one catalyst molecule for about 1000 epoxy monomers. During the initial polymerization process, most of the epoxy polymers

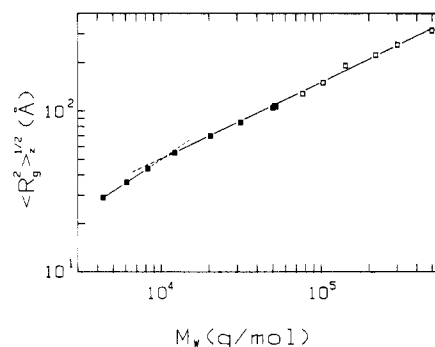


Figure 10. log-log plot of $\langle R_g^2 \rangle_z^{1/2}$ versus M_w . Solid squares denote SAXS measurements while hollow squares denote light scattering measurements. $M = k_R R_g^{d_R}$ with R_g and M expressed in units of Å and g/mol, respectively (fitting range, k_R , d_R): whole (13 points), 4.59 ± 0.41 , 2.00 ± 0.03 ; 3 low points, $(2.38 \pm 0.15) \times 10$, 1.55 ± 0.02 ; 10 higher points, 3.04 ± 0.33 , 2.07 ± 0.04 ; 9 higher points, 3.25 ± 0.76 , 2.06 ± 0.05 .

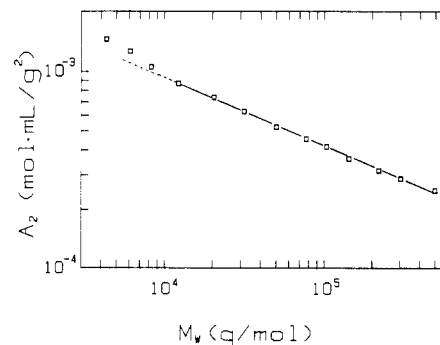


Figure 11. log-log plots of A_2 versus M_w from light scattering intensity measurements. $A_2 = k_A M_w^{\alpha_A}$ with A_2 and M in units of mol mL/g² and g/mol, respectively (fitting range, k_A , α_A): whole (13 points), $(3.02 \pm 0.31) \times 10^{-2}$, -0.37 ± 0.01 ; 10 higher points, $(2.19 \pm 0.13) \times 10^{-2}$, -0.34 ± 0.01 .

are relatively linear because the branching probability is fairly small.

From our light scattering intensity measurements we have also determined the second virial coefficient A_2 according to eq 1. Figure 11 shows a log-log plot of A_2 versus M_w . We have noted a curvature at low values of M_w , similar to the trend exhibited in Figure 10. By using

$$A_2 = k_A M_w^{\alpha_A} \quad (7)$$

we get $k_A = (3.02 \pm 0.31) \times 10^{-2}$ and $(2.19 \pm 0.13) \times 10^{-2}$ as well as $\alpha_A = -0.37 \pm 0.01$ and -0.34 ± 0.01 , respectively, with all 13 data points and the 10 higher molecular weight data points. We are not aware of experimental determinations for the constants k_A and α_A in highly branched polymers. However, experimental results on star-branch polymers suggest an α_A value of -0.37 for 12-arm and 18-arm polystyrene stars,¹⁴ in fairly good agreement with our findings.

The results of A_2 suggest that the lower M_w epoxy polymers are more swollen than the higher M_w epoxy polymers during the later stages of the curing process before the gel point. This observation agrees with our concept that during the initial polymerization stages, the epoxy polymer molecules are less branched. The smaller

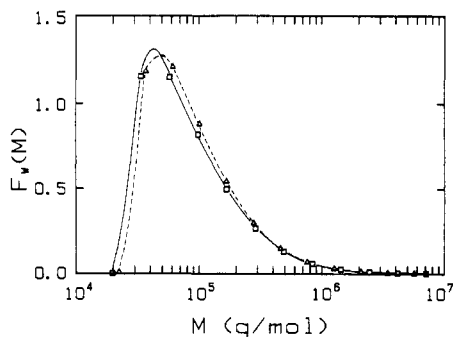


Figure 12. Typical molecular weight distribution of epoxy polymers during the curing process. Time correlation function data were taken at $\theta = 30^\circ\text{C}$ and $C = 7.19 \times 10^{-4}$ g/mL in MEK. We used \bar{D}^0 (cm^2/s) = $1.50 \times 10^{-4} M^{-0.482}$ with M expressed in g/mol to transform $G(\Gamma)$ versus Γ to $F_w(M)$ versus M yielding $M_w/M_n = 1.42 \times 10^5:5.89 \times 10^4$ g/mol = 2.41:1, as denoted by squares. If we take into account the changes of R_g/R_h ratio as a function of molecular weight, $\bar{D}^0 = 2.45 \times 10^{-4} M^{-0.526}$, $F_w(M)$ as denoted by triangles, yields $M_w/M_n = 1.42 \times 10^5:6.40 \times 10^4 = 2.22:1$.

degree of branching in the lower M_w epoxy polymers permits easier swelling of the polymer molecules. With increasing molecular weight, the polymer molecules become more highly branched and less swollen. The concept of fractal geometry is applicable because of the agreement between $d_R (= d_f) \sim 2.05$ over a substantial range of reaction time before the gel point, as shown in Table II and Figure 10.

5. Determination of Molecular Weight Distribution of Branched Epoxy Polymer in Solution. Before the gelation threshold, we can determine the molecular weight distribution (MWD) of branched epoxy polymers in solution using M_w from static light scattering, d_K from SAXS, and the normalized characteristic linewidth distribution function $G(\Gamma)$ from dynamic light scattering and Laplace inversion.^{3,5,15} In computing MWD, we have used M_w to determine k_D in the relation

$$M = k_D R_h^{d_h} \quad (8)$$

where we have taken into account the R_g and R_h differences as a function of molecular weight because of changes in the branching structure and assumed d_K to be the same for monodisperse and polydisperse branched epoxy polymers; i.e., the MWD is finite. Figure 12 shows a typical MWD determination for sample 10 with $M_w = 1.42 \times 10^5$ g/mol and $M_w/M_n = 2.41$.

6. Fractal Dimension beyond the Gelation Threshold. Beyond the gelation threshold, SAXS can be used to determine the fractal geometry of epoxy polymers as shown typically in Figure 13. For the present epoxy system, we still require immersion of the gel particles in MEK in order to increase the electron density difference. $d_f \sim 2.14 \pm 0.02$ and 2.13 ± 0.03 for $K \leq 1/30 \text{ \AA}^{-1}$ and $K \leq 1/20 \text{ \AA}^{-1}$, respectively. Further studies are underway.

IV. Conclusions

Branched polymer structures and macromolecular properties of epoxy polymers in solution can be investigated by using a combination of scattering techniques. By combining laser light scattering with small-angle X-ray

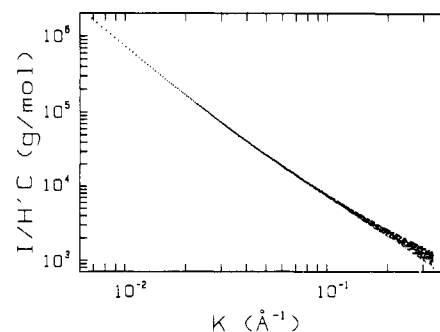


Figure 13. log-log plots of $I/H^2 C$ versus K . The epoxy gel was swollen in MEK. Least-squares fitting of 817 data points to $I \propto K^\alpha$ yields $\alpha = 2.14 \pm 0.02$ and 1.69 ± 0.05 for $K \leq 1/30 \text{ \AA}^{-1}$ and $1/30 \leq K \leq 1/4 \text{ \AA}^{-1}$, respectively.

scattering, we have developed a methodology to determine the molecular weight and the molecular weight distribution of random polymer structures before its gelation threshold during the curing process. Our method differs from the usual analytical technique such as size exclusion chromatography because we do not require fractionation of random branched polymers in solution but take advantage of the fractal geometry of random structures which can be determined by SAXS, provided that the MWD is finite.

Acknowledgment. We gratefully acknowledge support of this project by the U.S. Army Research Office (DAAG 2985 K0067) and the Department of Energy (DEFG0286ER45237A001 and DEFG0286ER45231A001).

Registry No. (DGEb)(CH) (copolymer), 113810-65-4.

References and Notes

- (1) See for example: Antoon, M. K.; Koenig, J. L. *J. Polym. Sci., Polym. Chem. Ed.* **1981**, *19*, 549, and references therein.
- (2) Mandelbrot, B. B. *Fractals, Form, Chance and Dimension*; Freeman: San Francisco, 1977. Mandelbrot, B. B. *The Fractal Geometry of Nature*; Freeman: New York, 1982.
- (3) Chu, B.; Wu, C.; Wu, D.-Q.; Phillips, J. C. *Macromolecules* **1987**, *20*, 2642.
- (4) May, C. A.; Tanaka, Y. *Epoxy Resins Chemistry and Technology*; Marcel Dekker: New York, 1973; p 683.
- (5) Chu, B.; Wu, C. *Macromolecules* **1987**, *20*, 93.
- (6) Chu, B.; Wu, D.-Q.; Wu, C. *Rev. Sci. Instrum.* **1987**, *58*, 1158.
- (7) Kratky, O.; Oelschlaeger, H. *J. Colloid Interface Sci.* **1969**, *31*, 490.
- (8) Sander, L. M. *Nature (London)* **1986**, *322*, 789; *Sci. Am.* **1986**, *256*, 94.
- (9) Meakin, P. "Fractal Aggregates and Thin Fractal Measures", to be submitted for publication.
- (10) Stanley, H. E. *J. Phys. A: Math. Gen.* **1977**, *A10*, L211.
- (11) Witten, T. A.; Sander, L. M. *Phys. Rev. Lett.* **1981**, *47*, 1400.
- (12) Mandelbrot, B. B. In *Fractals in Physics*; Proceedings of the 6th International Symposium of ICTP; Pietronero, L., Tosatti, Eds.; North-Holland: Amsterdam, 1986; pp 3, 17, and 21.
- (13) Daoud, M.; Joanny, J. F. *J. Phys. (Les Ulis, Fr.)* **1981**, *42*, 1359.
- (14) Huber, K.; Burchard, W.; Fetters, L. J. *Macromolecules* **1984**, *17*, 541.
- (15) Wu, C.; Buck, W.; Chu, B. *Macromolecules* **1987**, *20*, 98.
- (16) Cotton, J. P. *J. Phys., Lett.* **1980**, *41*, 231.
- (17) Daoud, M.; Family, F.; Jannink, G. *J. Phys., Lett.* **1984**, *45*, 199.
- (18) Schosseler, F.; Leibler, L. *Macromolecules* **1985**, *18*, 399.
- (19) Leibler, L.; Schosseler, F. *Phys. Rev. Lett.* **1985**, *55*, 1110.
- (20) Martin, J. E.; Ackerson, B. J. *Phys. Rev. A* **1985**, *31*, 1180.
- (21) Bouchard, E.; Delsanti, M.; Adam, M.; Daoud, M.; Durand, D. *J. Phys. (Les Ulis, Fr.)* **1986**, *47*, 1273.